RSC Advances

This is an *Accepted Manuscript*, which has been through the Royal Society of Chemistry peer review process and has been accepted for publication.

Accepted Manuscripts are published online shortly after acceptance, before technical editing, formatting and proof reading. Using this free service, authors can make their results available to the community, in citable form, before we publish the edited article. This *Accepted Manuscript* will be replaced by the edited, formatted and paginated article as soon as this is available.

You can find more information about *Accepted Manuscripts* in the Information for Authors.

Please note that technical editing may introduce minor changes to the text and/or graphics, which may alter content. The journal's standard Terms & Conditions and the Ethical guidelines still apply. In no event shall the Royal Society of Chemistry be held responsible for any errors or omissions in this *Accepted Manuscript* or any consequences arising from the use of any information it contains.

ROYAL SOCIETY OF CHEMISTRY

www.rsc.org/advances

Please do not adjust margins

Journal Name

ARTICLE

Arene-based Fluorescent Probes for the Selective Detection of Iron†

Received 00th January 20xx,
Accepted 00th January 20xx

DOI: 10.1039/x0xx00000x

www.rsc.org/

Pramod Kumar, Vijay Kumar, and Rajeev Gupta*

Pyridine-2,6-dicarboxamide based probes containing phenyl (**L1**), naphthyl (**L2**) and anthracenyl (**L3**) groups have been synthesized and screened towards Na^{+}, Mg^{2+}, Ca^{2+}, Cr^{3+}, Mn^{2+}, Mn^{3+}, Fe^{2+}, Fe^{3+}, Co^{2+}, Ni^{2+}, Cu^{2+}, Zn^{2+}, Hg^{2+}, Cd^{2+} and Pb^{2+} ions. Probes **L2** and **L3** exhibited remarkable sensing for Fe^{2+} and Fe^{3+} ions with **L3** being particularly selective. Collective studies comprising of Job's plot, Benesi-Hildebrand fitting, Stern-Volmer plot and detection limit display notable sensing ability of probe **L3** for Fe^{3+} as compared to Fe^{2+} ion. Competitive binding studies in presence of other metal ions further illustrated the high efficiency of **L3**. The probe **L3** binds to Fe^{3+} ion by forming a 1:1 complex with the apparent association constant (K_a) of $3.31x10^3$ M^{-1}. **L3**-Fe^{3+} system is shown to have potential applications in logic gate and cell imaging.

Introduction

Development of sensors for transition metal ions has received a great deal of attention due to relevance in a wide range of environmental and biological processes.[1,2] Iron is one of the physiologically most abundant transition metals in the living organism including humans. An average human adult contains approximately 3–5 g of iron and the total cellular concentration is approximately 50–100 μM.[3] Iron is involved in numerous cellular processes such as electron-transport, oxygen uptake, metabolism, and transcriptional regulation.[4,5] Biological iron almost exclusively exists in the ferrous (Fe^{2+}) and ferric (Fe^{3+}) state, although other oxidation states are routinely stabilized during catalytic cycles.[1a] Cells must carefully control iron levels, distribution, and speciation as excessive Fe^{3+} ion is responsible for several diseases including cancer, hepatitis, hemochromatosis, and dysfunction of vital organs.[6,7] Therefore, detection of iron especially in ferrous *versus* ferric form is immensely important and fluorescent probes are attractive tools to visualize its concentration and distribution.[8]

Many probes for iron exhibit "turn off" fluorescence response towards its binding.[9] However, a probe must be able to distinguish between the two oxidation states of iron. Because of the propensity of Fe^{2+} to oxidize to Fe^{3+} form under aerobic aqueous environment, it has been a challenge to design probes specific for ferrous ion.[1a] In last few years, several probes have been developed for the selective response to either Fe^{2+} or Fe^{3+} form or simply iron species.[9–18] Although most of these probes have only been used for modest applications in living cells, further developments including highly selective probes will undoubtedly result in better insights into iron cellular biology.

Scaffolds based on pyridine-2,6-dicarboxamide fragment have been widely used for anion sensing abilities.[19,20] Such a noteworthy feature is due to the desirable orientation of the hydrogen bonds in such scaffolds which assist in anion recognition. On the other hand, such scaffolds have also been used for coordinating assorted metal ions with notable structural and functional applications.[21,22] In this work, we have used three pyridine-2,6-dicarboxamide based probes (L1, L2 and L3) displaying the presence of a chelating cavity while also incorporating appended phenyl, naphthyl and anthracenyl groups as the fluorophores. Such fluorescent probes have been used for the selective binding of iron while displaying no interference from other metal ions. We also illustrate the application of one such probe in logic gate and in cell imaging.

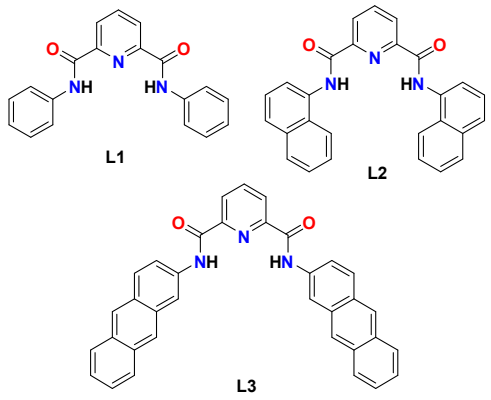

Scheme 1. Schematic representations of probes L1, L2 and L3.

Department of Chemistry, University of Delhi, Delhi-110007, India.
E-mail: rgupta@chemistry.du.ac.in; Fax: +91 - 11 - 2766 6605

†Electronic Supplementary Information (ESI) available: Figures for the FTIR, UV-vis, ESI-MS and NMR spectral studies, fluorescence spectral titration studies, detection limits; and a crystallographic table. CCDC 1424233. See DOI: 10.1039/x0xx00000x

RSC Advances Accepted Manuscript

Results and Discussion

Synthesis and characterization of probes

We have synthesized three pyridine-2,6-dicarboxamide based probes containing phenyl (L1), naphthyl (L2) and anthracenyl (L3) groups (Scheme 1). Probes L1 and L2 were synthesized according to the reported procedures[23,24] whereas L3 was synthesized by the coupling of pyridine-2,6-dicarboxylic acid with 2-aminoanthracene. FTIR spectrum of L3 shows N–H peak at 3270 cm^{-1} while O_{amide} stretch was noted at 1657 cm^{-1} (Fig. S1, ESI). The ^1H NMR spectrum shows N-H resonance at 11.3 ppm while aromatic protons appeared between 7.4-8.9 ppm (Fig. S2, ESI).The ESI^+ mass spectrum of probe L3 displays the molecular ion peak at 518.1868 for $[L3+H^+]$ (Fig. S3, ESI). The probes L1, L2, and L3 display absorption spectral maxima in THF at 300, 312 and 310 nm, respectively (Fig. S4, ESI).

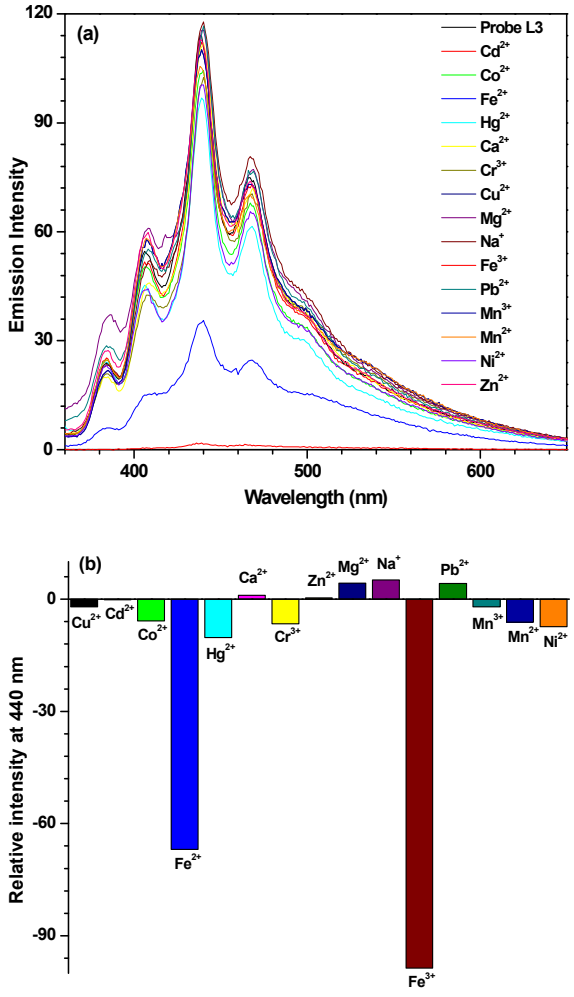

Fig. 1.(**a**) Emission spectrum of probe L3 (40 µM) in THF and after its interaction with 10 equiv. of assorted metal ions. (**b**) Bar diagram exhibiting change in emission intensity of probe L3 (40 µM) in THF after the addition of 10 equiv. of assorted metal ions.

Fluorescence studies

The photophysical properties of probes L1, L2 and L3 were examined in various solvents such as THF, MeOH, MeCN, DMF and CH_2Cl_2. Probe L1 showed a very poor emission at ca. 420 nm upon excitation at 300 nm at a very high concentration of 100 µM in MeOH (Fig. S5, ESI). Probe L2 exhibited a prominent emission at 408 nm after excitation at 335 nm (Fig. S6, ESI) whereas probe L3 displayed a significant emission at 440 nm after excitation at 340 nm (Fig. S7, ESI). Notably, both L2 and L3 displayed similar results in several solvents. It is clear that the presence of naphthyl and anthacenyl moieties in L2 and L3 is the major source of emission whereas phenyl ring in L1 is not an effective flurophore.

Addition of 10 equivalents of assorted metal ions, such as Na^+, Mg^{2+}, Ca^{2+}, Cr^{3+}, Mn^{2+}, Mn^{3+}, Co^{2+}, Ni^{2+}, Cu^{2+}, Zn^{2+}, Hg^{2+}, Cd^{2+} and Pb^{2+}, did not cause any appreciable change in the emission intensity of probe L2 (Fig. S8a, ESI) and L3 (Fig. 1a). On the other hand, introduction of Fe^{2+} and Fe^{3+} ion resulted in considerable quenching in the emission intensity (Fig. S8b (ESI) and 1b). A comparison of two probes, L2 and L3, illustrate that although both are selective for Fe^{2+} and Fe^{3+} ions; selectivity towards Fe^{3+} state is quite high (Fig. 2). Further, out of two probes, the performance of L3 is superior than that of L2.

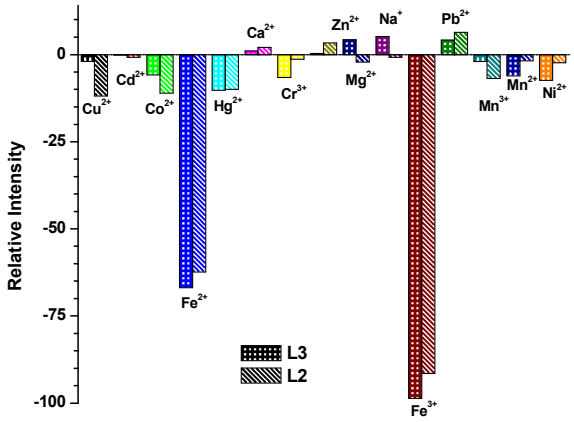

Fig. 2. Bar diagram exhibiting change in emission intensity of L2 (40 µM) and L3 (40 µM) in THF after addition of 10 equiv. of metal ions.

We then investigated the fluorescence quenching for both probes L2 and L3 by the incremental addition of 1-10 equivalents of Fe^{2+} and Fe^{3+} ions. For probe L2, addition of 10 equivalents of Fe^{2+} causes 62% quenching while Fe^{3+} resulted in 91% quenching (Fig. 3a). Importantly, probe L3 displayed nearly quantitative quenching on the addition of 10 equivalents of Fe^{3+}whereas a maximum of 65% quenching was noted for Fe^{2+}ion (Fig. 3b). To determine the extent of fluorescence quenching of probes L2 and L3 by Fe^{2+} and Fe^{3+} ions; Stern-Volmer constants (K_{SV}) were calculated.[25] The Stern-Volmer plots for probes L2 and L3 are shown in Fig. 3c and Fig. 3d, respectively whereas K_{SV} are presented in Table 1. The higher values of Ksv indicate strong quenching of probe L2 and L3 by Fe^{3+} ion when compared to Fe^{2+} ion. A further comparison exhibits a strong sensing ability of probe L3 towards Fe^{3+} ion as compared to Fe^{2+} ion.

RSC Advances Accepted Manuscript

This journal is © The Royal Society of Chemistry 20xx

Detection limits were also calculated both for L2 and L3 and the values are presented in Table 1 (see Fig. S9 and S10, ESI).[26] Both probes L2 and L3 showed good and excellent detection limits for Fe^{2+} and Fe^{3+} ions, respectively. It is clear from the Stern-Volmer constants and detection limits that the probe L3 shows a very high selectivity towards Fe^{3+} ion as compared to L2. Therefore, probe L3 was selected for further studies.

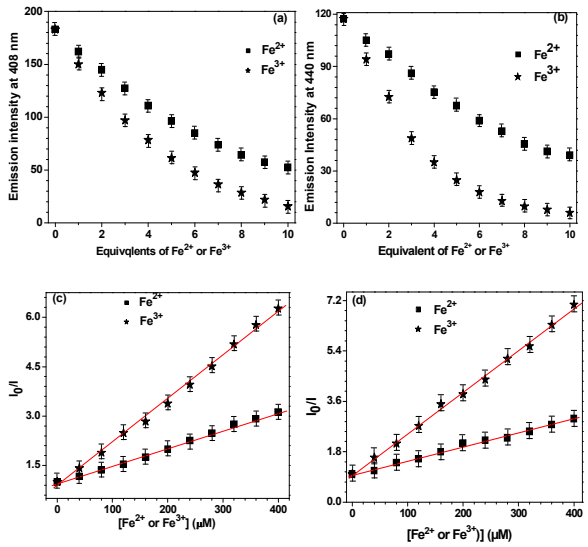

Fig. 3. Change in emission intensity with number of equivalents of Fe^{2+} versus Fe^{3+} ions for probe L2 (**a**) and L3 (**b**). Stern-Volmer plots for Fe^{2+} versus Fe^{3+} ions for probe L2 (**c**) and L3 (**d**). The points represent the mean ± the standard error of three independent sets.

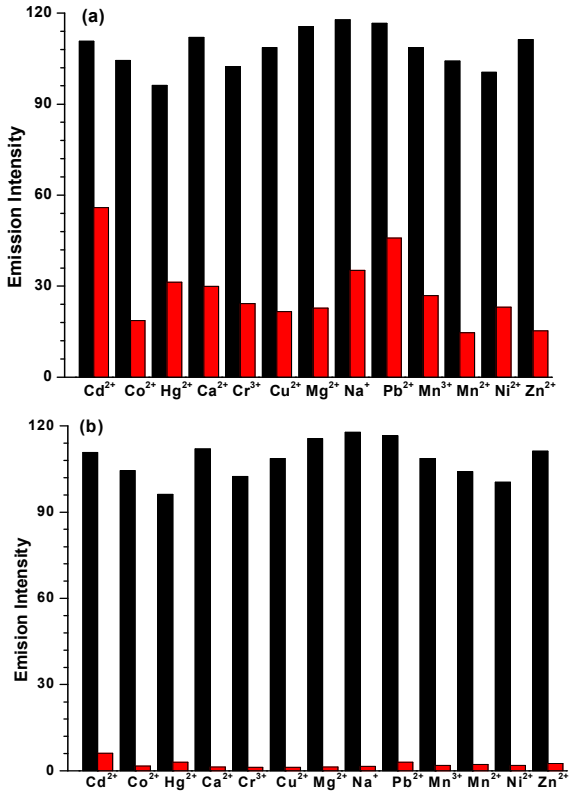

Fig. 4. Selectivity of Fe^{2+} versus Fe^{3+} ion in a THF solution containing probe L3 + metal ions (black bar) and L3 + metal ions + (**a**) Fe^{2+} (red bar) or (**b**) Fe^{3+} (red bar) as observed by the fluorescence spectral studies.

Table 1 Stern-Volmer constants (K_{SV}) and detection limits

Species	K_{SV} (M^{-1})	Detection limit (μM)
L2 + Fe^{2+}	5.49 x 10^3	08.54
L2 + Fe^{3+}	1.33 x 10^4	06.08
L3 + Fe^{2+}	4.94 x 10^3	11.27
L3 + Fe^{3+}	1.48 x 10^4	05.56

Selectivity studies

Competitive binding studies were performed to evaluate the interference from other metal ions such as Na^+, Mg^{2+}, Ca^{2+}, Cr^{3+}, Mn^{2+}, Mn^{3+}, Co^{2+}, Ni^{2+}, Cu^{2+}, Zn^{2+}, Hg^{2+}, Cd^{2+} and Pb^{2+} in the detection of Fe^{2+} and Fe^{3+} ions. For the competitive binding studies, equal concentrations of either Fe^{2+}or Fe^{3+} ion and other metal ions were taken with L3 in THF. Fig. 4 displays that among the metal ions tested, no metal ion effectively interferes with the Fe^{2+} ion and especially with Fe^{3+} ion. Therefore, probe L3 acts as an effective sensor for Fe^{2+} and Fe^{3+} ions even in presence of other metal ions.

Binding stoichiometry

The binding stoichiometry of anthracene-based probe L3 was investigated from Job's plot using fluorescence measurement.[27] Emission intensity was plotted against mole fraction of Fe^{3+}ion at 440 nm (Fig. 5a). The maximum in Job's plot clearly indicates a 1:1 binding stoichiometry of Fe^{3+} ion with probe L3. The binding stoichiometry was also investigated by the Benesi-Hildebrand plot which further supported a 1:1 stoichiometry.[28] An association constant, K_a, of 3.31x10^3 M^{-1} was determined by the ratio of intercept and slope in Benesi-Hildebrand plot (Fig. 5b). Notably, Benesi-Hildebrand plots either for 1:2 or 2:1 stochiometries between L3 and Fe^{3+} ion showed poor fit therefore again confirming a 1:1 stoichiometry (Fig. S11 and S11b, ESI).

The Job's plot and Benesi-Hildebrand method suggested a 1:1 stoichiometry and formation of a Fe-L3 complex. To gain a clear understanding of the formulation of Fe-L3 complex, we isolated the product in a reaction of L3 and $FeCl_3$ in THF (Complex **1**). This compound showed the disappearance of N–H stretches and bathochromic shift of O_{amide} frequency from 1657 (free L3) to 1602 cm^{-1} (Fig. S12, ESI). Both these features suggest the coordination of Fe(III) ion by the deprotonated N_{amide} groups within the pincer cavity.[22d,29] To further identify the nature of this compound, high-resolution ESI^+ mass spectrum was recorded which displays signals at *m/z* 701.4951 and at *m/z* 679.5123 corresponding to $[L3\text{-}2H+Fe^{3+}+Cl+THF+Na^+]^+$ and $[L3\text{-}2H+Fe^{3+}+Cl+THF+H^+]^+$, respectively (Fig. S13, ESI). Therefore, mass spectrum corroborates the findings from the FTIR spectrum which suggest the involvement of deprotonated L3 in binding. Based on the collective studies, we

RSC Advances Accepted Manuscript

propose a mononuclear formulation for the Fe-L3 complex (**1**) which is presented in Scheme 2.

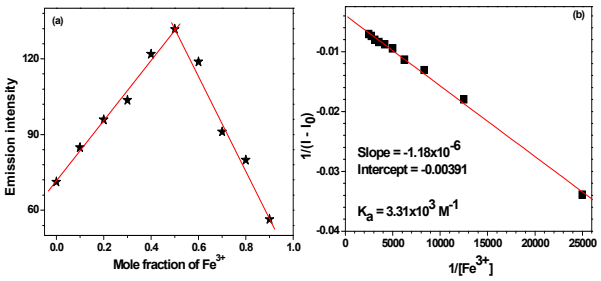

Fig. 5. (a) Job's plot of L3 and Fe^{3+} in THF. Total concentration of L3 and Fe^{3+} were maintained at 100 µM while the emission monitoring was done at 440 nm. (**b**) Benesi-Hildebrand plot for binding of Fe^{3+} ion with fluorescent probe L3.

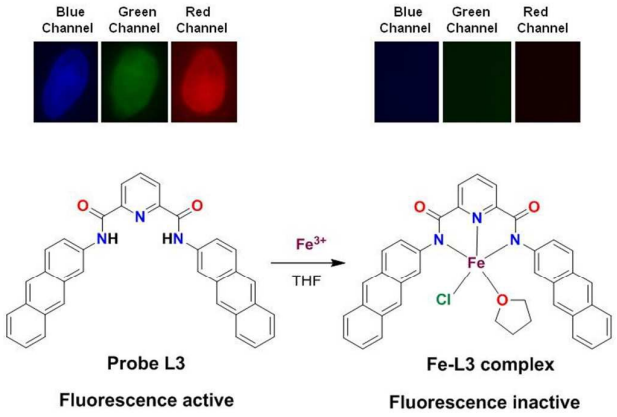

Scheme 2. Top: Fluorescent images of solid sample of probe L3 and Fe-L3 complex in different channels (blue, green and red). Bottom: A proposed Fe-L3 complex formed by the 1:1 stoichiometry of Fe^{3+} ion and L3.

Interestingly, when complex **1** was recrystallized from DMF/diethyl ether, a new compound, complex **2**, was obtained (Fig. S14, ESI). Complex **2** was crystallographically characterized and the molecular structure is shown in Fig. 6. The Fe(III) ion is coordinated by four deprotonated N_{amide} atoms in a tentative equatorial plane whereas two $N_{pyridyl}$ atoms occupy the axial positions. The Fe-N_{amide} and Fe-N_{py} bond lengths are similar to a related Fe(III) complex reported by Mukherjee and co-workers.[23] However, the Fe-N_{py} bond distances are larger than that observed for related structures.[30] The five-membered chelate based N_{amide}-Fe-N_{amide} bond angles range from 81.4 – 82.6° whereas N_{Py}-Fe-N_{Py} bond angle is 179.5 Å. To confirm whether the same compound (**2**) can be synthesized independently by a 2:1 reaction between the deprotonated probe L3 and $FeCl_3$ led to the isolation of **2** in high yield. We also recorded the emission spectrum of complex **2** and compared it either with a mixture of probe L3 and Fe^{3+} ion or isolated complex **1**. As anticipated, complex **2** is fluorescence inactive, very similar to that of complex **1** or emission of L3 in presence of Fe^{3+} ion (Fig. S15, ESI).

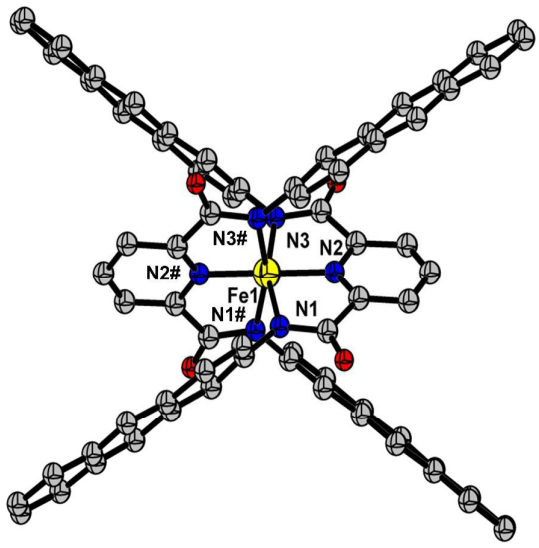

Fig. 6. Ball and stick structure of the anionic part of complex **2**; hydrogen atoms and tetrabutyl ammonium ion has been omitted for clarity. Selected bond distances (Å): Fe1-N1= 1.8618, Fe1-N2 =1.9415, Fe1-N3 = 1.9617. Selected bond angles (°): N1-Fe1-N2 = 82.6, N1-Fe1-N3 = 81.4, N2-Fe1-N3 = 164.0, N2-Fe1-N2# = 179.5.

Reversibility and Logic gate applications

In order to develop a reversible probe for sensing Fe^{3+} ion, attempts were made to remove Fe^{3+} ion from the Fe-L3 complex. EDTA is known to have a strong tendency to chelate a variety of metals including Fe^{3+} ion and form a $[Fe–EDTA]^-$ complex.[31] Fig. 7a displays that Fe^{3+} ion quenches the fluorescence intensity of probe L3 nearly quantitatively. However, addition of EDTA restores the fluorescence intensity of the probe L3 to nearly initial value.[32] Further addition of Fe^{3+}ionagain led to quantitative quenching. Such a fact establishes a reliable nature of probe L3. We have converted the sensing of Fe^{3+} ion in presence and absence of EDTA into logic gates which are used in several electronic devices such as molecular switches and keypads.[33,34] We assumed that Fe^{3+} ion and EDTA are used as the inputs while the fluorescence intensity is used as an output. Emission intensity at 100 was taken as threshold frequency at 440 nm. Therefore, emission intensity above this threshold value gives OUT = 1 and below this OUT = 0. Consequently, these inputs (Fe^{3+} ion and EDTA) generate a truth table for Or gate as illustrated in Fig. 7b.

RSC Advances Accepted Manuscript

This journal is © The Royal Society of Chemistry 20xx

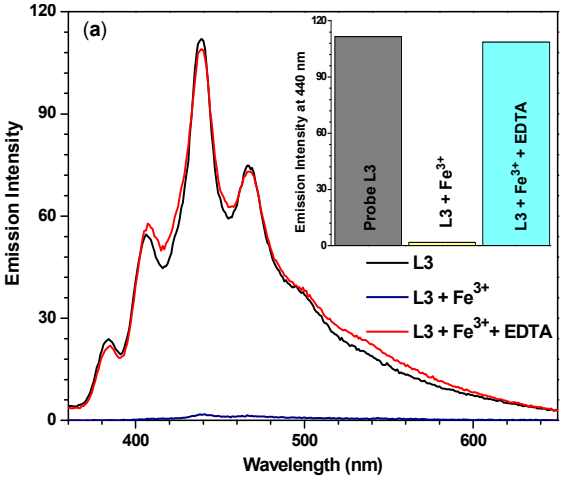

(b) OR gate and Truth Table

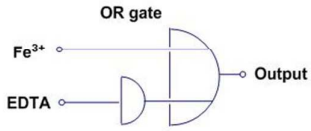

Fe^{3+}	EDTA	Output
0	0	1
0	1	1
1	0	0
1	1	1

Fig. 7. (a) Emission spectra and bar diagram for change in emission intensity (inset) of L3 (40 μM) in presence of Fe^{3+} ion (10 equiv.) and EDTA (20 equiv.) in THF-water mixture.[32] (**b**) Logic functions and truth table by change in emission intensity of L3 upon input of Fe^{3+}ion and EDTA.

Cytotoxicity assays

As the probe L3 showed highest selectivity for Fe^{3+} ion out of three probes L1 – L3; we selected it for the biological cell imaging applications.[35] Before going to cell imaging, we attempted to ascertain the viability of cells towards probe L3 in absence and presence of Fe^{3+} ion. Therefore, cytotoxicity activity of L3 against HEK-293, Hep-2, and L929 cell lines was investigated in comparison with the widely used anti-cancer drug cis-platin under the identical conditions by using MTT assay.[36] The in-vitro cytotoxicity against HEK-293, Hep-2, and L929 cell lines is presented in Table 2. The anti-proliferative effects were tested using the MTT assay and were quantified in terms of IC_{50} values; lower the IC_{50} value, higher the anti-proliferative activity. The results show that probe L3 is less cytotoxic against all three HEK-293, Hep-2, and L929 cell lines as compared to probe L3 in presence of Fe^{3+} ion. Further, probe L3 in absence as well as in presence of Fe^{3+} ion showed significantly lower cytotoxicity as compared to cis-platin on all three tested cell lines. These studies advocate that the probe L3 can be used for the cell imaging in absence as well as presence of Fe^{3+} ion without causing any damage to the cell lines.

Table 2 IC_{50} values of in vitro cytotoxicity assay for HEK-293, Hep-2, and L929 cells.

Species	IC_{50} (μM)		
	HEK-293	Hep-2	L929
Probe L-3	108.24	117.35	94.26
Probe L-3 + Fe^{3+}	78.59	83.68	69.38
Cis-platin	13.38	12.62	11.05

Fluorescence cell imaging

Cell cytotoxicity assay showed that the probe L3 has very low cytotoxicity; hence, can be used for the intracellular imaging.The application of probe L3 as an intracellular Fe^{3+} ion sensor was performed with L929 cells by fluorescence imaging. Fluorescence microscopic images of L929 cells for the blue, green and red channels are presented in Fig. 8. Examination of these images clearly illustrate that the probe L3 (40 μM) provides intense fluorescence inside the cells after its incubation for 90 min (Fig. 8a). Notably, incubation of probe L3 in presence of $FeCl_3$ for 90 min, considerably quenches the fluorescence by the formation of Fe-L3 complex inside the cells (Fig. 8b). Further addition of $FeCl_3$ quenches the fluorescence emission completely (Fig. 8c). We have already established that probe L3 coordinates with Fe^{3+} ion to form Fe-L3 complex which is fluorescent inactive. It can, therefore, be concluded that the probe L3 provides an effective mean to measure Fe^{3+} ion concentration within the living cells. Importantly, solid samples of probe L3 also display a similar quenching on exposure to ferric ion (cf. top portion of Scheme 2) thus suggesting wider applications.

Conclusions

In this report, a series of pincer-cavity based probes containing phenyl (L1), naphthyl (L2) and anthracenyl (L3) groups has been synthesized and studied. Probes L2 and L3 selectively detected iron both in +2 and +3 oxidation states. Notably, probe L3 afforded the best results when compared to L1 and L2. Fluorescence quenching, competitive binding studies, Stern-Volmer plots and detection limit advocated strong sensing ability of probe L3 for the Fe^{3+} ion as compared to Fe^{2+} ion. A 1:1 binding stoichiometry between L3 and Fe^{3+} ion was established with Job's plot with an association constant (K_a) of 3.31×10^3 M^{-1}. Reversibility with EDTA demonstrated an intricate application in logic gate devices. Probe L3 was successfully used for the fluorescence based cell imaging and the results are supported with cell viability studies. Although iron selective probes have not been thoroughly investigated and optimized as compared to other metals; present results provide a strategy of developing pincer-cavity based selective probes and may find applications in tracking labile iron in living cells and tissues.

RSC Advances Accepted Manuscript

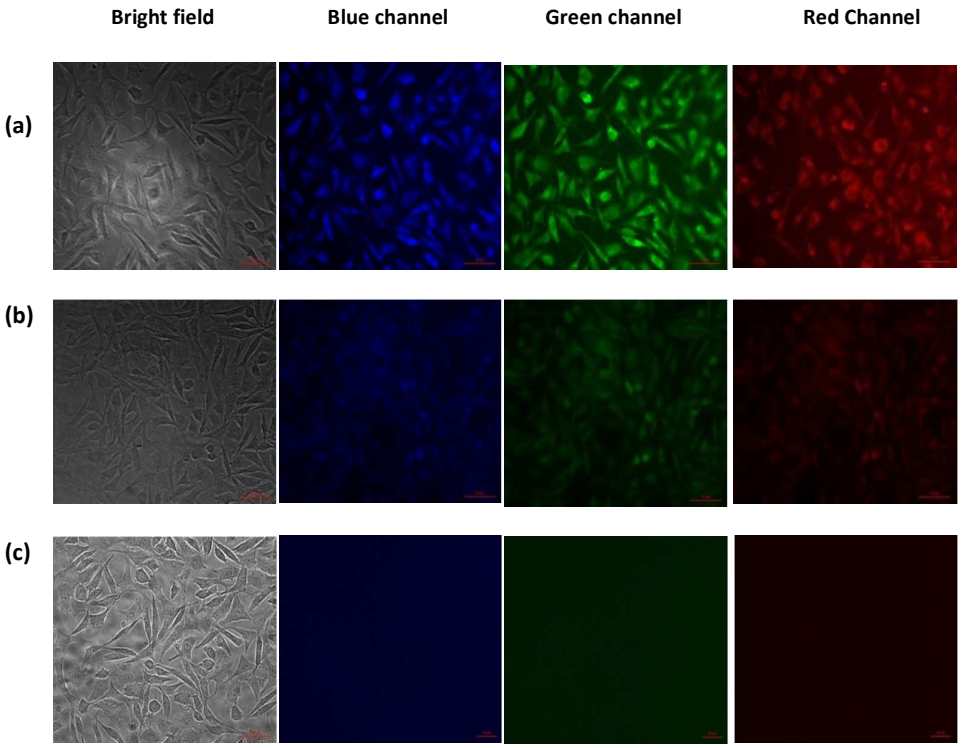

Figure 8. Fluorescent microscopic images (40x) of L929 cells after incubation for 90 minutes in growth medium: (a) Cells treated with probe L3 (40 µm); (b) Cells treated with probe L3 (40 µM) and $FeCl_3$ (400 µM); (c) Cells treated with probe L3 (40 µm) and $FeCl_3$ (1 mM).

Experimental Section

Materials and methods

All reagents and metal salts were used as received without further purifications. HPLC grade solvents were used for the UV-vis and fluorescence measurements. Probes L1 and L2 were synthesised as per the literature reports.[23,24]

Syntheses of Probe L3

Pyridine-2,6-dicarboxylic acid (1.0 g, 0.0059 mol) and 2-aminoanthracene (1.196 g, 0.0119 mol) were taken in 25 mL pyridine and refluxed with stirring for 30 min at 120 °C. $P(OPh)_3$ (3.877 g, 0.0125 mol) was added drop-wise to the aforementioned reaction mixture. The reaction mixture was finally stirred at 80 °C for 12 h. After cooling to room temperature, the reaction mixture was poured into ice-cold water that caused precipitation of the product, which was filtered, washed with water followed by ethanol and dried in vacuum. Yield: 2.48 g (80%). Anal. calc. for $C_{35}H_{23}N_3O_2$: C, 81.22; H, 4.48; N, 8.12. Found: C, 81.24; H, 4.50; N, 8.15. FTIR spectrum (cm^{-1}): 3270 (N–H), 1657 (C=O). UV/Vis (THF): λ_{max} (ε, M^{-1} cm^{-1}) = 280 (74220), 310 (46200), 325 (42820), 375 (22120), 395 (15400).ESI^+-MS spectrum (CH_3CN, *m/z*): 518.1868 for $[L3+H^+]$. ^1H NMR spectrum (400 MHz, DMSO-d^6): δ = 11.31 (s, 2H), 8.81 (s, 2H), 8.59 (s, 4H),8.52-8.47 (d, J = 8.04 Hz, 2H), 8.40-8.34 (t, J = 8.56 Hz, 1H), 8.23-8.18 (d, J = 9.32 Hz, 2H), 8.11-8.06 (d, J = 7.92 Hz, 4H), 8.05-8.00 (d, J = 9.16 Hz, 2H) 7.57-7.45 (m, 4H). ^{13}C NMR spectrum (100 MHz, DMSO-d^6): 162.59 (C4), 149.40 (C3), 135.68 (C5), 132.28 (C1), 131.96 (C9), 131.31 (C13), 129.46 (C15), 129.39 (C16), 128.66 (C8), 128.36 (C14), 126.54 (C17), 126.32 (C2), 126.07 (C12), 126.03 (C10), 125.81 (C11), 122.77 (C6), 117.04 (C7).

Synthesis of Complex 1

Probe L3 (0.10 g, 0.193 mmol) was dissolved in THF (5 mL) followed by the drop-wise addition of a solution of $FeCl_3$ (0.312 g, 1.93 mmol) dissolved in 5 mL THF. The reaction mixture was stirred for 2 h at room temperature. The solvent was removed under reduced pressure and the crude compound thus obtained was washed with diethyl ether and dried. FTIR spectrum (cm^{-1}): 1602 (C=O), 1454, 1346. UV/Vis spectrum (THF): λ_{max} (ε, M^{-1} cm^{-1}) = 330 (84270), 373 (46250), 395 (24900). ESI-MS spectrum (THF, *m/z*): 679.5123 for $[L3-2H+Fe+Cl+THF+H^+]$ and 701.4951 for $[L3-2H+Fe+Cl+THF+Na^+]$.

Synthesis of Complex 2

Probe L3 (0.10 g, 0.193 mmol) was dissolved in THF (5 mL) and treated with solid NaH (0.092 g, 0.386 mmol). The resulting solution was stirred for 10 min at room temperature followed by the drop-wise addition of a solution of $FeCl_3$ (0.031 g, 0.193 mmol) dissolved

RSC Advances Accepted Manuscript

 This journal is © The Royal Society of Chemistry 20xx

in 5 mL THF. After 15 min, tetrabutyl ammonium bromide (.062 g, 0.193 mmol) was added and the reaction mixture was stirred for 2 h at room temperature. The solvent was removed under the reduced pressure and the crude compound thus obtained was washed with diethyl ether and dried. Reddish brown crystals were obtained by the vapour diffusion of diethyl ether into a DMF solution of compound within one week. Yield: 0.16 g (74%).Anal. calc. for $C_{70}H_{42}N_6O_4FeNa$: C, 75.75; H, 3.81; N, 7.57. Found: C, 75.72; H, 3.83; N, 7.54. FTIR spectrum (cm^{-1}): 1601 (C=O), 445(7460). 1456, 1347. UV/Vis (THF): λ_{max} (ε, M^{-1} cm^{-1}) = 375 (21560), 395 (17020),

Physical Methods

Elemental analysis data were obtained by Elementar Analysen Systeme GmbH Vario EL-III instrument. The ^1H and ^{13}C NMR spectra were recorded with a JEOL 400 MHz instrument. The FTIR spectra (Zn–Se ATR) were recorded with a Perkin-Elmer Spectrum-Two spectrometer. The absorption spectra were recorded with a Perkin-Elmer Lambda 25 spectrophotometer. Fluorescence studies were performed with a Cary Eclipse Fluorescence Spectrometer. ESI-MS mass spectra were obtained with Q-TOF LC/MS mass spectrometer of Agilent.

UV-Visible and Fluorescence Measurements

All stock solutions of L1, L2 and L3 (1 mM) and metal salts (10 mM) of Na^+, Mg^{2+}, Ca^{2+}, Cr^{3+}, Mn^{2+}, Mn^{3+}, Fe^{2+}, Fe^{3+}, Co^{2+}, Ni^{2+}, Cu^{2+}, Zn^{2+}, Hg^{2+}, Cd^{2+} and Pb^{2+} ions were prepared in THF. All UV-vis and fluorescence spectra were recorded with a 1.0 cm path length cuvette.

Determination of Stern-Volmer constant (K_{SV}) and detection limit

Fluorescence titrations were further evaluated using the Stern–Volmer equation [equation (1)].[25]

$$I_o/I = 1+K_{SV}[Q] \quad (1)$$

Where I_o is the emission intensity in the absence of quencher, I is the emission intensity in the presence of quencher (Q) and K_{SV} is the Stern–Volmer constant.

The detection limit was calculated using equation (2),

$$\text{Detection limit: } 3\sigma/k \quad (2)$$

where σ is the standard deviation of a blank measurements and k is the slope of a plot of fluorescence intensity versus metal ion concentration.[26]

Determination of the binding stoichiometry and the apparent association constant K_a

The binding stoichiometry of Fe^{3+} with L3 was determined by the Job's plot.[27] The fluorescence intensity at 440 nm was plotted against mole fraction of probe L3 at constant concentration. The apparent association constant (K_a) of Fe-L3 complexes was determined by the Benesi-Hildebrand equation.[28] The association constant K_a was calculated graphically by plotting $1/(I-I_0)$ against $1/[Fe^{3+}]$.

$$1/(I-I_0) = 1/\{K_a(I_0 - I\text{min})[Fe^{3+}]\} + 1/(I_0 - I\text{min}) \quad (3)$$

Where I is the fluorescence intensity of L3 in presence of Fe(III) ion at 440 nm, I_0 is the intensity of L3 in absence of Fe^{3+} ion and I_{min} is the minimum fluorescence intensity in presence of Fe^{3+} ion. The plot $1/(I-I_0)$ vs. $1/[Fe^{3+}]$ were linearly fitted and the K_a value was obtained from the slope and intercept of the line.

In vitro cytotoxicity assay

The cytotoxicity potential of the fluorescent probe L3 in absence and presence of Fe^{3+} was evaluated by the MTT (3-(4,5-dimethylthiazol-2-yl)-2,5-diphenyltetrazolium bromide) assay against HEK-293, Hep-2, and L929 cells.[36] HEK-293, Hep-2, and L929 cells ($1x10^4$) were seeded on 96-well plates in growth medium and incubated at 37 °C in an atmosphere containing 5% CO_2. After incubation of 24 h, testing solutions of serial concentrations were added to each well and incubated for next 24 h. The tested solutions were made in DMEM medium with DMSO for better solubility while the final concentration of DMSO was 1%. At the end of each treatment, cell viability was assessed according to the manufacturer's instructions. Briefly, after discarding the medium, MTT labelling mixture (5 mg/mL) was added to the cells and incubated for 2 h at 37 °C. The media with MTT were removed and 100 µM of DMSO was added to dissolve the insoluble formazon. Absorbance values were determined on Fluostar optima (BMG Labtech, Germany) microplate reader at 570 nm. The percentage of inhibition was calculated as:

$$\frac{\text{Mean OD of vehicle treated cells} - \text{Mean OD of treated cells}}{\text{Mean OD of vehicle treated cells}} \times 100$$

The IC_{50} (50 % inhibitory concentration) values were obtained by the nonlinear regression, using the Graph Pad Prism version 5 program. All experiments were independently repeated at least three times, with triplicate samples for each treatment.

Fluorescence cell imaging

In vitro studies with probe L3 in presence as well as in absence of Fe^{3+} were carried out with L929 cells (murine cancer cells). L929 cells were cultured in DMEM medium supplemented with 1 % streptomycin as antibiotic, and incubated in CO_2 incubator at 37 °C. Cells were seeded at a density of 2.0×10^5 cells per well in six well plate and were incubated at 37 °C for 12 h. Cells were incubated with probe L3 (40 µM) in phosphate buffer saline (PBS) for 90 min. In another set of experiment, cells were incubated with probe L3 (40 µM) and $FeCl_3$ (400 µM and 1mM). After 90 min incubation, cells were washed with PBS three times to remove the traces of probe L3. Finally the cells were fixed with 4% paraformaldehyde solution. Stained slides were observed and acquired the image in Upright Microscope (Axio Imager 2.2, Carl Zeiss, Germany).

RSC Advances Accepted Manuscript

X-ray Crystallography

Single crystals suitable for the X-ray diffraction studies were grown by the vapor diffusion of diethyl ether into a dimethyl formamide solution of complex **2**. The intensity data were collected at 298 K with an Oxford XCalibur CCD diffractometer equipped with graphite monochromatic Mo-*K*α radiation (*λ* = 0.71073 Å).[37] Data reduction was performed with the CrysAllisPro program (Oxford Diffraction ver. 171.34.40). The structure was solved using the direct methods using SHELXS-97[38] program and refined on F^2 using all data by full matrix least-squares procedures with SHELXL-97[39] within the OLEX-2 suite.[40] The hydrogen atoms were placed at the calculated positions and included in the last cycles of the refinement. All calculations were done using the WinGX software package.[41] Crystallographic data collection and structure solution parameters are summarized in Table S1 (ESI).

Acknowledgements

RG acknowledges the Council of Scientific and Industrial Research (CSIR), New Delhi and the University of Delhi for the financial support. PK thanks UGC, New Delhi for the Dr. D.S. Kothari Postdoctoral fellowship. Authors thank the CIF-USIC at this university for the instrumental facilities and crystallographic data collection and Dr. Arun Kumar (IIT Delhi) for technical assistance in cell imaging work.

Notes and references

1 (a) K. P. Carter, A. M. Young, and A. E. Palmer, *Chem. Rev.*, 2014, **114**, 4564−4601; (b) X.Chen, T. Pradhan, F. Wang, J. S. Kim, and J. Yoon, *Chem. Rev.*, 2012, **112**, 1910-1956; (c) M. E. Jun, B. Roy, and K. H. Ahn, *Chem. Commun.*, 2011, **47**, 7583–7601; (d) J. Du, M. Hu, J. Fan, and X. Peng, *Chem. Soc. Rev.*, 2012, **41**, 4511–4535.

2 (a) H. N. Kim, W. X. Ren, J. S. Kim, and J. Yoon, *Chem. Soc. Rev.*, 2012, **41**, 3210-3244; (b) T. Nagano, Y. Gabe, Y. Urano, K. Kikuchi, and H. Kojima, *J. Am. Chem. Soc.*, 2004, **126**, 3357–3367; (c) T. Terai, Y. Urano, S. Izumi, H. Kojima, and T. Nagano, *Chem. Commun.*, 2012, **48,** 2840–2842.

3 R. C. Hider and X. Kong, *Dalton Trans.*, 2013, **42**, 3220-3229.

4 (a) E. Beutler, *Science*, 2004, **306**, 2051−2053; (b) P. L. Llewellyn, P. Horcajada, G. Maurin, T. Devic, N. Rosenbach, S. Bourrelly, C. Serre, D. Vincent, S. Loera-Serna, Y. Filinchuk, and G. Ferey, *J. Am. Chem. Soc.*, 2009, **131**, 13002−13008.

5 (a) S.Dai, C. Schwendtmayer, P. Schurmann, S. Ramaswamy, and H. Eklund, *Science*, 2000**, 287**, 655−658; (b) A. Atkinson and D. R. Winge, *Chem. Rev.*, 2009, **109**, 4708−4721; (c) C. D. Kaplan and J. Kaplan, *Chem. Rev.*, 2009, **109**, 4536−4552; (d) E. C. Theil and D. J. Goss, *Chem. Rev.*, 2009, **109**, 4568-4579.

6 (a) D. Galaris, V. Skiada, and A. Barbouti, *Cancer Lett.*, 2008*,* **266**, 21−29; (b) N. K. Desai, G. B. Kolekar, and S. R. Patil, *New J. Chem.*, 2014, **38**, 4394-4403.

7 (a) B. Halliwell, *J.Neurochem.,*1992, **59**, 1609−1623; (b) E. D. Weinberg, *Eur. J. Cancer Prev.*, 1996, **5**, 19−36.

8 P. Das, N. B. Chandar, S. Chourey, H. Agarwalla, B. Ganguly, and A. Das, *Inorg. Chem.*, 2013, **52***,* 11034-11041.

9 (a) C. X. Yang, H. B. Ren, and X. P. Yan, *Anal. Chem.*, 2013, **85**, 7441-7446; (b) J. Brandel, N. Humbert, M. Elhabiri, I. J. Schalk, G. L. Mislin, and A. M. Albrecht-Gary, *Dalton Trans.*, 2012, **41**, 2820-2834.

10 (a) Y. Ma, W. Luo, P. J. Quinn, Z. Liu, and R. C. Hider, *J. Med. Chem.*, 2004, **47**, 6349−6362; (b) X. Qu, Q. Liu, X. Ji, H. Chen, Z. Zhou, and Z. Shen, *Chem. Commun.*, 2012, **48**, 4600−4602; (c) Q. X. Yao, J. L. Sun, K. Li, J. Su, M. V. Peskov, and X. Zou, *Dalton Trans.*, 2012, **41**, 3953−3955.

11 (a) B. Wang, J. Hai, Z. Liu, Q. Wang, Z. Yang, and S. Sun, *Angew. Chem. Int Ed.*, 2010, **49**, 4576−4579; (b) S. K. Sahoo, D. Sharma, R. K. Bera, G. Crisponi, and J. F. Callan, *Chem. Soc. Rev.*, 2012, **41**, 7195−7227.

12 (a) B. Bodenant, F. Fages, and M.-H. Delville, *J. Am. Chem. Soc.*, 1998, **120**, 7511−7519; (b) M. Xu, S. Wu, F. Zeng, and C. Yu, *Langmuir*, 2010, **26***,* 4529–4534

13 (a) J. Mao, L. Wang, W. Dou, X. Tang, Y. Yan, and W. Liu, *Org. Lett.*, 2007, **9**, 4567–4570; (b) Y. Xiang, and A. Tong, *Org. Lett.*, 2006, **8**, 1549–1552.

14 S. Fakih, M.Podinovskaia, X. Kong, U. E. Schaible, H. L. Collins, and R. C. Hider, *J. Pharm. Sci.*, 2009, **98**,2212−2226.

15 (a) H. Weizman, O. Ardon, B. Mester, J. Libman, O. Dwir, and Y. Hadar, Y. Chen, *J. Am. Chem. Soc.*, 1996, **118**, 12368−12375; (b) W. D. Chen, W. T. Gong, Z. Q. Ye, Y. Lin, and G. L. Ning, *Dalton Trans*., 2013, **42**, 10093−10096; (c) M. H. Lee, T. V. Giap, S. H. Kim, Y. H. Lee, C. Kang, and J. S. Kim, *Chem. Commun.*, 2010, **46**, 1407−1409.

16 (a) G. Mukherjee and K. Biradha, *Chem. Commun.*, 2012, **48**, 4293− 4295; (b) T. K. Prasad, D. H. Hong, and M. P. Suh, *Chem. Eur. J.*, 2010, **16**, 14043−14050; (c) L. W. Mi, H. W. Hou, Z. Y. Song, H. Y. Han, and Y. T. Fan, *Chem. Eur. J.*, 2008, **14**, 1814−1821.

17 Z. Yang, M. She, B. Yin, J. Cui, Y. Zhang, W. Sun, J. Li, and Z. J. Shi, *J.Org. Chem.*, 2012**, 77**, 1143-1147.

18 (a) S. K. Sahoo, D. Sharma, R. K. Bera, G. Crisponi, and J. F. Callan, *Chem. Soc. Rev.*, 2012, **41**, 7195-7227; (b) H. N. Kim, M. H. Lee, H. J. Kim, J. S. Kim, and J. Yoon, *Chem. Soc. Rev.*, 2008, **37**, 1465−1472.

19 A. Dorazco-Gonzalez, M. F. Alamo, C. Godoy-Alcantar, H. Hopfl, and A. K. Yatsimirsky, *RSC Adv.*, 2014, **4,** 455–466.

20 A. Dorazco-Gonzalez, H. Hopfl, F. Medrano, and A. K. Yatsimirsky, *J. Org. Chem.*, 2010, **75**, 2259–2273.

21 (a) P. J. Donoghue, A. K. Gupta, D. W. Boyce, C. J. Cramer, and W. B. Tolman, *J. Am. Chem. Soc.*, 2010, **132**, 15869–15871; (b) P. Pirovano, A. M. Magherusan, C. McGlynn, A. Ure, A.Lynes, and A. R. McDonald, *Angew. Chem. Int. Ed.*, 2014, **53**, 5946 –5950; (c) P. J. Donoghue, J. Tehranchi, C. J. Cramer, R.Sarangi, E. I. Solomon, and W. B. Tolman, *J. Am. Chem. Soc.*, 2011, **133**, 17602–17605; (d) A. K. Patra and R. Mukherjee, *Inorg. Chem.*,1999, **38**,1388-1393; (e) A. K. Singh, V. Balamurugan, and R. Mukherjee, *Inorg. Chem.*, 2003, **42**,6497-6502.

22 (a) D. Huanga, O. V. Makhlynetsb, L. L. Tan, S. C. Lee, E.V. Rybak-Akimova, and R. H. Holm, *Proc. Nat. Acad. Sci.*, 2011, **108**,1222–1227; (b) X. Zhang, D. Huang, Y.-S. Chen, and R. H. Holm, *Inorg. Chem.*, 2012, **51**, 11017−11029; (c) D. Huang and R. H. Holm, *J.*

RSC Advances Accepted Manuscript

 This journal is © The Royal Society of Chemistry 20xx

Am. Chem. Soc., 2010, **132**, 4693–4701; (d) D. Bansal, G. Kumar, G. Hundal, and R. Gupta, *Dalton Trans.* 2014, **43**, 14865–14875.

23 M. Ray, D Ghosh, Z. Shirin, and R. Mukherjee *Inorg. Chem.* 1997, **36***,* 3568-3572.

24 K. Ghosh, S. Kumar, R. Kumar, and U. P. Singh, *J. Organomet. Chem.*, 2014, **750**, 169-175.

25 A. Ganguly, B. K. Paul, S. Ghosh, S. Kar, and N. Guchhait, *Analyst*, 2013, **138**, 6532-6541.

26 C. Liang, W. Bu, C. Li, G. Men, M. Deng, Y. Jiangyao, H. Sun, and S. Jiang, *Dalton Trans.* 2015**, 42**, 1827–1833.

27 A. Senthilvelan, I. Ho, K. Chang, G. Lee, Y. Liu, and W. Chung, *Chem. Eur. J.*, 2009, **15**, 6152-6160.

28 (a) H. A. Benesi and J. H. Hildebrand, *J. Am. Chem. Soc.*, 1949, **71**, 2703-2707; (b) R. B. Singh, S. Mahanta, and N. Guchhait, *J. Mol. Struct.* 2010, **963**, 92-97.

29 S. Srivastava, M. S. Dagur, and R. Gupta, *Eur. J. Inorg. Chem.* 2014, 4966–4974

30 D. S. Marlin, M. M. Olmstead, and P. K. Mascharak, *Inorg. Chem.*, 1999, **38***,* 3258-3260.

31 EM. A. Zaitoun and C. T. Lin, *J. Phys. Chem. B*, 1997, **101**, 1857-1860.

32 EDTA was added to a THF-water (40%, v/v) solution of probe L3 and Fe^{3+} ion. Under these conditions, emission spectrum of probe L3 and its interaction with Fe^{3+} ion was similar as noted in neat THF.

33 (a) M. Kumar, A. Dhir, and V. Bhalla, *Org. Lett.*, 2009, **11**, 2567-2570; (b) V. Bhalla, Roopa, and M. Kumar, *Org. Lett.*,2012,**14**, 2802-2805.

34 (a) D.Margulies, C. E. Felder, G. Melman, and A. Shanzer, *J. Am. Chem.Soc.*, 2007, **129**, 347-354;(b) B.Rout, P. Milko, M. A. Iron, L. Motiei, and D. Margulies, *J. Am. Chem.Soc.*, 2013, **135**, 15330-15333.

35 For cell imaging, 1% DMSO-water (v/v) mixture and DMEM buffer was used. Under these conditions, the emission spectrum of probe L3 and its interaction with Fe^{3+} ion was similar as noted in neat THF.

36 T. Mosmann, *J. Immunol. Methods.*, 1983, **65**, 55-63.

37 *CrysAlisPro*, v. 1.171.33.49b, Oxford Diffraction Ltd., 2009.

38 G. M. Sheldrick, ActaCrystallogr., Sect. A: Found. Crystallogr. 2008, **64**, 112−122.

39 Sheldrick, G. M. SHELXL-97, Programs for X-ray Crystal Structure Refinement; University of Göttingen: Gottingen, Germany, 1997.

40 Dolomanov, O. V.; Bouhis, L. J.; Gildea, R. J.; Howard, J. A. K.; Puschmann, H. J. Appl. Crystallogr. 2009, **42**, 339−341.

41 Farrugia, L. J. J. Appl. Crystallogr. 1999, **32**, 837– 838.

RSC Advances Accepted Manuscript

Graphical Abstract

Synopsis: Amide based probes containing phenyl (**L1**), naphthyl (**L2**) and anthracenyl (**L3**) groups were screened towards a large number of metal ions. Probes **L2** and **L3** display notable sensing for Fe^{2+} and Fe^{3+} ions with **L3** being particularly selective. **L3**-Fe^{3+} system has been shown to have potential applications in logic gates and cell imaging.

Pictorial:

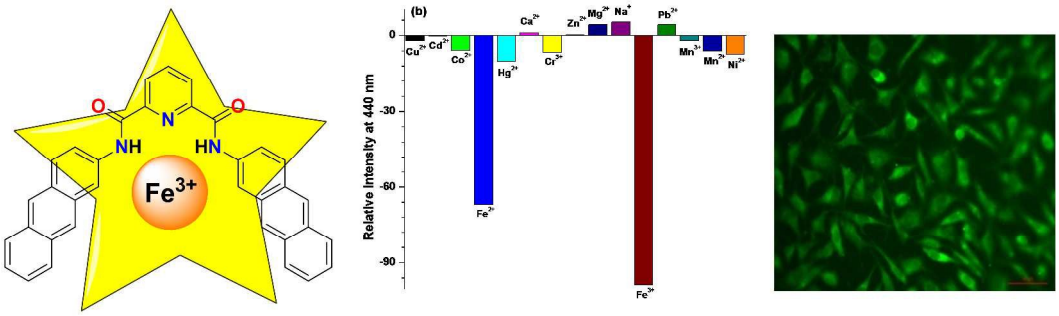

RSC Advances Accepted Manuscript